HHS Public Access

Author manuscript

Neurobiol Dis. Author manuscript; available in PMC 2020 December 01.

Published in final edited form as:

Neurobiol Dis. 2020 December ; 146: 105130. doi:10.1016/j.nbd.2020.105130.

TDP-43 and Tau Oligomers in Alzheimer's Disease, Amyotrophic Lateral Sclerosis, and Frontotemporal Dementia

Mauro Montalbano[1,2], **Salome McAllen**[1,2], **Filippa Lo Cascio**[1,2], **Urmi Sengupta**[1,2], **Stephanie Garcia**[1,2], **Nemil Bhatt**[1,2], **Anna Ellsworth**[1,2], **Eric A. Heidelman**[3], **Omar D. Johnson**[3], **Samantha Doskocil**[4], **Rakez Kayed**[1,2,*]

[1]Mitchell Center for Neurodegenerative Diseases, University of Texas Medical Branch, Galveston, Texas, 77555, USA

[2]Departments of Neurology, Neuroscience, and Cell Biology, University of Texas Medical Branch, Galveston, Texas, 77555, USA

[3]School of Medicine, University of Texas Medical Branch, UTMB, Galveston, Texas, 77555, USA

[4]Neuroscience Summer Undergraduate Research Program, NSURP Program 2018

Abstract

Proteinaceous aggregates are major hallmarks of several neurodegenerative diseases. Aggregates of post-translationally modified transactive response (TAR)-DNA binding protein 43 (TDP-43) in cytoplasmic inclusion bodies are characteristic features in frontotemporal dementia (FTD) and amyotrophic lateral sclerosis (ALS). Recent studies have also reported TDP-43 aggregation in Alzheimer's disease (AD). TDP-43 is an RNA/DNA binding protein (RBP) mainly present in the nucleus. In addition to several RBPs, TDP-43 has also been reported in stress granules in FTD and ALS pathologies. Despite knowledge of cytoplasmic mislocalization of TDP-43, the cellular effects of TDP-43 aggregates and their cytotoxic mechanism(s) remain to be clarified. We hypothesize that TDP-43 forms oligomeric assemblies that associate with tau, another key protein involved in ALS and FTD. However, no prior studies have investigated the interactions between TDP-43 oligomers and tau. It is therefore important to thoroughly investigate the cross-seeding properties and cellular localization of both TDP-43 and tau oligomers in neurodegenerative

*Corresponding Author at: Rakez Kayed, PhD University of Texas Medical Branch Medical Research Building Room 10.138C 301 University Blvd Galveston, TX 77555-1045, rakayed@utmb.edu.

Author Contributions

Conceptualization, M.M. and R.K.; Methodology, M.M. and R.K.; Investigation, M.M., S.M., F.L.C., S.D., E.H., O. J., and R.K.; Writing – Original Draft, M.M. and O.J.; Writing – Review & Editing, all authors; Funding Acquisition, R.K.; Resources, R.K.; Supervision, M.M. and R.K.

Availability of data and materials

The datasets used and/or analyzed in this current study are available from the corresponding author. All existing and new antibodies, reagents are available for sharing with scientists at nonprofit institutions worldwide who request them according to NIH guidelines and within institutional guidelines and common practice.

Conflict of Interest: None

Declaration of Interests

The authors declare no competing interests.

diseases. Here, we demonstrate the effect of tau on the cellular localization of TDP-43 in WT and P301L tau-inducible cell models (iHEK) and in WT HEK-293 cells treated exogenously with soluble human recombinant tau oligomers (Exo-rTauO). We observed cytoplasmic TDP-43 accumulation o in the presence of tau in these cell models. We also studied the occurrence of TDP-43 oligomers in AD, ALS, and FTD human brain tissue using novel antibodies generated against TDP-43 oligomers as well as generic TDP-43 antibodies. Finally, we examined the cross-seeding property of AD, ALS, and FTD brain-derived TDP-43 oligomers (BDT43Os) on tau aggregation using biochemical and biophysical assays. Our results allow us to speculate that TDP-43/tau interactions might play a role in AD, ALS, and FTD.

Keywords

TDP-43; Tau; Aggregation; Oligomer; Tauopathies; Neurodegeneration

Introduction

Amyotrophic lateral sclerosis (ALS) and frontotemporal dementia (FTD) are neurodegenerative disorders that share genetic, molecular, and clinical features (Ferrari et al., 2011; Mandrioli et al., 2020). Proteomics approaches have revealed that both are characterized by ubiquitinated and phosphorylated protein inclusions in affected neurons (Hedl et al., 2019; Neumann et al., 2006). Post-mortem brain tissue from ALS and FTD patients were shown to contain ubiquitinated and phosphorylated RNA-binding protein (RBP) transactive response (TAR)-DNA binding protein 43 (TDP-43) (Gao et al., 2018; Ling et al., 2013)

The single-stranded RNA and DNA binding protein TDP-43 is a versatile molecule that participates in various cellular processes but is mainly involved in RNA metabolism (Butti and Patten, 2019). TDP-43 is primarily localized in the nucleus but also shuttles to the cytoplasm (Ederle and Dormann, 2017; Prasad et al., 2019), where it is incorporated into stress and RNA granules (Mandrioli et al., 2020; Monahan et al., 2016) or droplets (Gasset-Rosa et al., 2019), maintaining phase separation through its low-complexity domain (Guenther et al., 2018). TDP-43 is involved in several steps of RNA metabolism such as transcription, translation, mRNA transport and stabilization, microRNA production, and long non-coding RNA processing (Ratti and Buratti, 2016).

TDP-43 stress granule formation is caused by pathological conditions and cellular stress (Chen and Cohen, 2019). In ALS, TDP-43 forms large inclusion bodies composed of aberrant proteins with various post-translational modifications such as hyper-phosphorylation, polyubiquitination, and proteolytic cleavage (Berning and Walker, 2019). Other RBP complexes such as heterogeneous nuclear ribonucleoproteins, FUS, TIA-1, Matr3, Ataxin2, Musashi1, and Musashi2 and their aggregation dynamics play an important role in neurodegenerative diseases (Montalbano et al., 2019; Nussbacher et al., 2015; Nussbacher et al., 2019; Sengupta et al., 2018b). Large RBP complexes that mis-localize to the cytoplasm have neurotoxic effects. Additionally, mislocalization and accumulation of TDP-43 in cytoplasmic inclusion bodies is a prominent feature of ALS and FTD that leads

to a loss of functional TDP-43 within the nucleus (Gasset-Rosa et al., 2019). TDP-43 was recently shown to disrupt nuclear pores in ALS/FTD brain tissues (Chou et al., 2018), providing new mechanistic insights into neurodegenerative pathogenesis.

Clinicopathological research has established that the two most important pathological hallmarks associated with cognitive impairment in patients with ALS or FTD are TDP-43 and the microtubule-binding protein tau (Takeda, 2018). The study of TDP-43 proteinopathies is a relatively new field. Interestingly, some of the paradigms observed in tauopathies also seem to be applicable to TDP-43 proteinopathies, including specific genetic modifiers (Chornenkyy et al., 2019).

To address the molecular mechanisms of TDP-43/tau interaction and its role in neurodegenerative diseases, we analyzed the biochemical characteristics and cellular localization of TDP-43 species, focusing on oligomeric forms. To study pathological TDP-43, we characterized TDP-43 oligomers (TDP-43Os) with standard biochemical methods using anti-TDP43O antibodies generated in-house. To investigate TDP-43 seeding properties, we cross-seeded recombinant monomeric tau protein (2N4R) with TDP-43Os isolated from AD, ALS, and FTD brain tissues (brain-derived TDP-43Os, BDT43Os). BDT43Os represent all the oligomeric TDP-43 species isolated from diseased human brain tissue. To examine the effects of tau oligomers on TDP-43 aggregation and cellular localization, we treated HEK-293 cells with recombinant tau oligomers (Exo-rTauO) and tau monomers (Exo-rTauM). We observed different patterns of high molecular weight (HMW) TDP-43 species between the cytoplasm and nuclei, indicating potential compartment-dependent deposition of TDP-43. We simultaneously detected increased cytoplasmic TDP-43Os using our newly developed antibodies termed TDP-43-Oligo01 and TDP-43-Oligo02. Interestingly, Exo-rTauO did not significantly affect HEK-293 cell expression of the *TARDBP* gene that encodes the TDP-43 protein, suggesting that tau modulates the aggregation but not the expression of endogenous TDP-43. We isolated and examined the cross-seeding properties of AD, ALS and FTD BDTDP-43Os with tau protein by biochemical and biophysical assays. Collectively, our data demonstrate that TDP-43/tau interactions might be crucial crosstalk in the pathogenesis of several proteinopathies. Based on these observations, we propose that TDP-43Os may serve as a nucleation site for tau aggregates. We also propose that tau oligomers modulate TDP-43 aggregation state and cellular localization.

Materials and Methods

Preparation of TDP-43Os.

Recombinant WT TDP-43 was purified using the method previously described (Johnson et al., 2009). Briefly, pCOLD- TDP 43 was transformed into *E. coli* cells. The proteins were purified over a nickel-nitrilotriacetic acid column. Purified protein was quantified using Bicinchoninic acid assay (Thermo Scientific, #23235). Oligomers of recombinant full-length WT TDP-43 were prepared following previously published protocol (Choksi et al., 2014). Briefly, 30 μM of TDP-43 was mixed with hexafluoroisopropanol and 1X sterile phosphate-buffered saline (PBS). This solution was stirred with a Teflon coated stir bar for 48 h inside fume hood at room temperature (RT).

Three different peptide sequences of human full length TDP-43 protein (FGNQGGFG, GAAIGWGS, and GVRLVEGI) were synthesized by Dr. Jai Rudra's laboratory. The peptide fragments were dissolved in 1X PBS at equimolar concentration. The mixed solution was then stirred at 500 rpm with a Teflon-coated micro stir bar for 48 h inside the fume hood at RT.

Preparation of recombinant tau species.

Recombinant tau protein (Tau-441 (2N4R) MW 45.9 kDa) was expressed and purified as previously described (Margittai and Langen, 2004; Margittai and Langen, 2006). The tau pellet was treated with 8M urea followed by overnight dialysis against 1X PBS (pH 7.4). Tau concentrations were measured using Pierce™ BCA protein assay kits (Thermo Fisher Scientific; 23225) and normalized to 1 mg/mL by adding 1X PBS. Aliquots of tau monomer (TauM) in PBS were stored at −20°C. Each 300 μL of tau stock (0.3 mg) was added to 700 μL of 1X PBS and incubated for 1 h on an orbital shaker at RT. After shaking, the resulting tau oligomers (TauO) were purified by fast protein liquid chromatography (FPLC, Superdex 200 Increase 10/300 column, Amersham Biosciences). TauM aliquots were incubated with heparin (15 kDa) (1:5 molar ratio) to prepare tau fibrils (TauF) at 37°C on an orbital shaker at a speed of 30 rpm for 5 days as previously described (Ghag et al., 2018).

Tau oligomer labeling and cell treatments.

TauO were produced and characterized using previously published protocols (Gerson et al., 2017). TauO labeling was conducted as follows: 1 mg of Alexa Fluor™ 568 NHS Ester (Invitrogen, #A20003) was dissolved in 0.1 M sodium bicarbonate to yield a final concentration of 1 mg/mL. The dye was then incubated with TauO in a 1:5 (w/w) ratio. The mixture was rotated overnight at 4°C on an orbital shaker. The following day, the solution was centrifuged (30 min, 15,000 x g) using 10-kDa Amicon Ultra-0.5 Centrifugal Filter Units to remove unbound dye. The oligomers were then washed with 1X PBS until clear flow-through solution was obtained. The filter compartment was then flipped and centrifuged to collect the concentrate. The oligomers were reconstituted to their original volume. TauO-568 was resuspended in complete Dulbecco's minimum essential medium (DMEM) to obtain final 0.5 μM and 2 μM concentration solutions. The cells were treated with TauO-568 mixed in DMEM for 1 h at a controlled temperature of 37°C and 5% CO_2. After the medium was removed, the cells were collected for cytoplasmic and nuclear protein fractioning and immunofluorescence (IF) assays.

Seeding assay.

Recombinant Tau 4R monomers were seeded with BDT43Os from AD, FTD, or ALS brain tissues as previously described (Lo Cascio et al., 2020; Puangmalai et al., 2020). The BDT43O-TauM mixture was made at a ratio of 1:100 (w/w) with gentle agitation at RT for 2 days. After seeding, aliquots were taken and immediately used for immunoblotting (IB) using Tau5 and Tau 13 antibodies as well as atomic force microscopy analysis for quality control (data not shown). Total protein concentrations were determined using Pierce™ BCA protein assay kits (Thermo Scientific; 23225) and stored at −20°C until use.

Generation of TDP-43O-specific polyclonal antibodies.

TDP-43Os mixed with Freund's complete adjuvant were used as antigen to immunize two New Zealand white rabbits (Pacific Immunology Corp. Ramona, CA). The immunization process was carried out according to the protocol approved by Pacific Immunology, where each rabbit was given a dose of 200 μg of antigen as the first injection. This was followed by three booster doses of 100 μg each. Sera from the immunized rabbits were tested in biochemical assays. The sera with the highest antigen binding and more specificity were affinity-purified in a protein A column and used for further analyses.

Cell cultures and treatments.

Three different cell lines were used in this study: HEK-293 control, iHEK overexpressing wild-type (WT) tau and iHEK overexpressing mutated P301L tau (Dr. Laura Blair). They were maintained in DMEM supplemented with 10% fetal bovine serum (FBS) at 37°C with 5% CO_2. To induce overexpression of WT and mutant tau, the iHEK cells were treated with 1 μg/mL of tetracycline (Tet) for 24 h in FBS-depleted DMEM (Gibco™ LS11965118, Fisher Scientific). After 24 h, cells were collected and immediately washed twice with medium to remove excess Tet and then stained. Cell detachment was performed with Trypsin (Gibco™ Trypsin-EDTA, 0.25% Phenol red, LS25200114 Fisher Scientific) for 3 min in an incubator and then centrifuged at 1000 rpm for 5 min. Cell pellets were harvested and collected for cell fractionation (Montalbano et al., 2019).

RNA isolation and quantitative reverse transcription polymerase chain reaction (RT-qPCR).

Total RNA from iHEK cells was extracted using TRIzol reagent following the established protocol (Montalbano et al., 2020a). RNA samples were quantified using a Nanodrop Spectrophotometer (Nanodrop Technologies) and qualified by analysis on an RNA Nano chip using the Agilent 2100 Bioanalyzer (Agilent Technologies); only samples with high-quality total RNA were used (RIN: 7.5–10.0). cDNA synthesis was performed with 0.5 or 1 μg of total RNA in a 20-μl reaction using the reagents in the Taqman Reverse Transcription Reagents Kit from Life Technologies (#N8080234). Q-PCR amplifications (performed in duplicate or triplicate) were done using 1 μl of cDNA in a total volume of 20 μl using the iTaq Universal SYBR Green Supermix (Bio-Rad #1725125). The final primer concentration was 300 nM. Relative RT-qPCR assays were performed with 18S RNA or another housekeeping gene as a normalizer. Absolute analysis was performed using known amounts of synthetic transcript from the gene of interest. All PCR assays were run in the ABI Prism 7500 Sequence Detection System. The list of primers used is in the supplemental material section.

IB and cytoplasmic/nuclear fractioning.

IB analyses were performed with iHEK cell samples. Approximately 10 μg of protein preparations were loaded on precast NuPAGE 4–12% Bis-Tris gels (NP0335BOX, Invitrogen) for sodium dodecyl sulfate-polyacrylamide gel electrophoresis (SDS-PAGE) analyses. Gels were subsequently transferred onto nitrocellulose membranes and blocked overnight at 4°C with 10% nonfat dry milk. Membranes were then probed for 1 h at RT with pTDP-43 (1:1000, TIP-PTD-M01 CosmoBio), total TDP43 (1:1000, ab109535 Abcam),

TDP-43O-specific antibodies (TDP-43-Oligo01, TDP-43-Oligo02, 1:1000, in-house), Pan-Tau (Tau13, 1:10,000, MMS-520R Covance), Tau 5 (1:5000, 806402 BioLegend), glyceraldehyde 3-phosphate dehydrogenase (GAPDH, 1:1000, ab9485 Abcam), LaminB1 (1:1000, ab133741 Abcam), and Histone3 (1:1000, ab201456 Abcam) antibodies diluted in 5% nonfat dry milk. Immunoreactivity was detected with a horseradish peroxidase (HRP)-conjugated anti-rabbit immunoglobulin G (IgG, 1:10,000, NA934 GE Healthcare). P-TDP43, Tau13, and Tau 5 immunoreactivity were detected using an anti-mouse IgG (1:10,000, NA931 GE Healthcare) diluted in 5% milk. ECL plus (K-12045-D50, GE Healthcare) was used to visualize protein bands. LaminB1/Histone3 and GAPDH were used to normalize and quantify nuclear and cytoplasmic proteins, respectively. The compartment extraction was conducted with Qproteome Cell Compartment Kits (Qiagen, #37502); nuclear, cell membrane, and cytoplasmic proteins were isolated and preserved for IB analysis.

Human brain tissue harvesting.

Frontal cortex brain tissues from AD (n=3), FTD (n=2), ALS (n=3), and age-matched control subjects (n=3) were received as frozen blocks from the Institute for Brain Aging and Dementia at UC Irvine following approval by the Institutional Ethics Committee. Brain tissues were homogenized in 1X PBS mixed with a protease inhibitor cocktail (Roche, #11836145001) and phosphatase inhibitor (Sigma, #04906837001) at 1:3 (w/v) dilution of brain:PBS. Samples were then centrifuged at 10,000 x g for 10 min at 4°C. The supernatants (PBS-soluble fractions) were aliquoted, snap-frozen, and stored at −80°C until use. The pellets were re-suspended in Sarkosyl solution at a final concentration of 1% with stirring for 1 h at RT and then centrifuged at 100,000 x g for 30 min at 4°C. Sarkosyl-soluble fractions (PBS-insoluble fractions) were aliquoted, snap-frozen, and stored at −80°C until use. Human brains characteristics are summarized in Table 1 in the supplemental material section.

IF and confocal microscopy.

IF assays were performed with frozen sections of AD, ALS, and FTD cortex brain tissues. Frozen sections were fixed in chilled methanol then blocked in 5% normal goat serum for 1 h. Sections were then washed three times with 1X PBS and incubated overnight with TDP43-Oligo-01 (1:300), TDP43-Oligo-02 (1:300), A11 (1:300), OC (1:1000), Tau13 (1:1000), Tau 5 (1:300), and 6E10 (1:300) at 4°C. After washing three times with 1X PBS (10 min each), sections were then incubated for 1 h with goat anti-mouse IgG Alexa Fluor 488 and anti-rabbit Alexa Fluor 568 (1:700, Thermo Fisher Scientific), as appropriate. They were then washed, stained, and mounted with ProLong™ Gold Antifade Mountant with DAPI (Invitrogen, P36962). The single-frame images and Z-stacks for 3D rendering and orthogonal view were collected using a Zeiss LSM880 Confocal Microscope equipped with a Nikon 63x oil immersion objective and processed with Zeiss Lite Black Software. The human brain slides were imaged using standard Nikon GFP, FITC, and DAPI filters. Images were processed and analyzed with ImageJ software (National Institutes of Health, NIH). Z-Stacks (0.5-μm step size) were obtained and stored. All co-localization Pearson correlation coefficient (PCC) values were obtained from 10 scatter plots and profile plots using NIH

ImageJ software. A researcher blinded to treatment groups performed the image acquisition and analyses from randomly chosen regions of interest (ROIs).

BDT43O isolation and characterization.

The PBS-soluble fractions of AD, FTD, and ALS brain homogenates were immunoprecipitated (IP'ed) with TDP43-Oligo01 antibody. The Pierce™ Co-Immunoprecipitation Kit (Thermo Scientific, #26149) was used following the manufacturer's guidelines. Briefly, amine-reactive resin was coupled with the TDP-43-Oligo01 antibody, which suitable for IP, followed by incubation with brain homogenates (PBS-soluble fractions). Bound proteins were eluted in 0.1 M glycine (pH 2.8), and the final pH was adjusted to 7.0 by adding 1 M Tris-HCl (pH 8). Isolated fractions were subjected to buffer exchange and finally collected in sterile PBS followed by IB characterization. The total protein concentrations were measured with bicinchoninic acid protein assays (Micro BCA Kit, Pierce).

Dot blot.

Dot blot assays to detect tau oligomers were performed as previously described (Lo Cascio and Kayed, 2018a). Briefly, 1.5 μl of sample was applied onto nitrocellulose membranes and then blocked with 10% nonfat milk in Tris-buffered saline with Tween 0.01% (TBS-T) overnight at 4°C. Membranes were then probed with either TDP-43 oligo antibody (1:1000) or pTDP-43 antibody (1:1000) diluted in 5% nonfat milk for 1 h at RT. Membranes were then incubated with HRP-conjugated IgG anti-rabbit (1:10,000) to detect TDP-43O immunoreactivity. Blots were then washed three times in TBS-T before ECL plus (GE Healthcare) was used for signal detection.

Filter trap assay.

Filter trap assays were performed using a Bio-Dot SF Microfiltration Apparatus (Bio-Rad) as previously described (Lo Cascio et al., 2019). Briefly, 1 μg of sample was applied to nitrocellulose membranes that were pre-wetted with TBS-T using a vacuum-based bio-slot apparatus. Membranes were then blocked with 10% nonfat milk in TBS-T overnight at 4°C. The next day, membranes were probed with the oligomer-specific TDP-43 antibodies, TDP-43-Oligo01 (1:1000), TDP-43-Oligo02 (1:1000), and pTDP-43 (1:1000) diluted in 5% nonfat milk for 1 h at RT. Membranes were then incubated with HRP-conjugated IgG anti-rabbit (1:10,000) or anti-mouse (1:10,000) secondary antibody. Membranes were washed three times in TBS-T before ECL plus (GE Healthcare) was used for signal detection.

Cross seeding and Proteinase K (PK) digestion assay.

TauM were seeded with BDT43O at a 1:70 w/w ratio. The samples were then rotated on an orbital shaker as previously described (Bittar et al., 2019; Lo Cascio et al., 2020) and characterized using standard protocols (Sengupta et al., 2018a). Tris-HCl and NaCl were added to each sample so that the final concentrations were 100 mM and 5 mM, respectively. Samples were then treated with 0, 1, or 2 μg/mL PK enzyme (p-2308, Sigma) and incubated at 37°C for 1 h. The enzymatic reaction was stopped by adding 4X SDS-PAGE loading

buffer (NuPAGE LDS sample buffer, Invitrogen) followed by incubation at 95°C for 5 min. Samples were then used for IB analysis or stored at −80°C.

Bis-ANS and thioflavin T (ThT) fluorescence assays.

Fluorescence spectroscopy was performed as previously described (Lo Cascio et al., 2020; Lo Cascio and Kayed, 2018b; Lo Cascio et al., 2019; Sengupta et al., 2020). Samples were prepared by adding 2 μL of BDT43O (0.3–0.5 μg/μL) or control samples (TauO, TauM, and TauF) and 248 μL of 10 μM bis-ANS (4,4′-dianilino-1,1′-binaphthyl-5,5′-disulfonic acid, B153, Invitrogen), prepared in 100 mM glycine-NaOH buffer (pH 7.4) in a clear-bottom, 96-well black plate. Each experiment was performed in triplicate. Bis-ANS fluorescence intensity was measured at an emission wavelength of 520 nm upon excitation at 380 nm. For ThT assays, samples were prepared using 2 μL of BDT43O (0.3–0.5 μg/μL) or control samples (TauO, TauM, and TauF) and 248 μL of 5 μM ThT (T3516, Sigma) dissolved in 50 mM glycine-NaOH buffer (pH 8.5). Each experiment was performed in triplicate. ThT fluorescence intensity was recorded at an emission wavelength of 490 nm upon excitation at 440 nm using a Polar Star Omega plate reader (BMG Labtech). Fluorescence spectra of the following solutions were measured as negative controls for both dyes (bis-ANS and ThT): dye alone and dye + vehicle. Each reading was corrected for the corresponding background fluorescence.

Statistical analysis.

All *in vitro* experiments were performed in at least three biological replicates. All data are presented as means ± SD and were analyzed using GraphPad Prism Software 7.0. Statistical analyses included Student's t-test or one-way analysis of variance (ANOVA) followed by Tukey's multiple comparisons test. Column means were compared using one-way ANOVA with treatment as the independent variable. Group means were compared using two-way ANOVA with factors on treatment. When ANOVA showed a significant difference, pairwise comparisons between group means were examined by Tukey's and Dunnett's multiple comparison tests.

Results

Exo-rTauO alter TDP-43 localization in HEK-293 cells.

To study the effect of rTauO on TDP-43 intracellular localization and aggregation, we performed cell fractioning of HEK-293 cells treated with 0.5 and 2.0 μM rTauO. We also studied distinct TDP-43 oligomeric species and their intracellular levels using antibodies recognizing phosphorylated and oligomeric forms of TDP-43. IB of nuclear and cytoplasmic fractions was performed with a commercial TDP-43 antibody (Figure 1A and 1B, respectively). The commercial antibody predominantly recognized the monomeric form of TDP-43 (mTDP-43) (Figure 1A). We observed a significant increase in nuclear TDP-43 compared to HMW forms of TDP-43 (>50 kDa) in the nuclear fraction of rTauO-treated cells. There was no significant difference in cytoplasmic levels of monomeric and HMW forms of TDP-43 after rTauO incubation (Figure 1B). LaminB1 and GAPDH were used as controls for loading and purity of subcellular fractionations of nuclear and cytoplasmic fractions, respectively. Interestingly, we observed different HMW TDP-43 banding patterns

in the two fractions, indicating a compartment-dependent distribution of HMW TDP-43 forms (Supplementary Figure 1A–D). We observed four main bands at ~75 kDa and above in the nucleus, whereas the cytoplasm had a robust band at ~250 kDa that was not detected in the nuclei. We also evaluated pTDP-43 levels using a commercial antibody that recognizes the form of TDP-43 phosphorylated at Ser409/410 (Clone 11–9). Similar to Figure 1A, the level of nuclear monomeric pTDP-43 was significantly increased in HEK-293 cells treated with rTauO at both concentrations (Figure 1C). We also observed a non-significant increase in HMW p-TDP43 in the nuclei and cytoplasm, indicating an overall enhancement of pTDP-43 forms in the presence of rTauO (Figure 1D). In summary, we detected both phosphorylated and non-phosphorylated mTDP-43 in the nuclei, as well as a general increase in HMW p-TDP43 forms in both the nuclei and cytoplasm of HEK-293 cells. These results suggest that exogenous TauO modulates monomeric TDP-43/pTDP-43 localization, inducing a general increase of HMW TDP-43 in both cell compartments.

Exo-rTauO induces cytoplasmic accumulation of TDP-43O in HEK-293 cells.

We developed and tested in-house anti-oligomeric TDP-43 antibodies in HEK-293 cells treated with Exo-rTauO (Figure 2). The characterization of anti-oligomeric TDP-43 antibodies is shown in Supplementary Figure 2. The TDP-43O-specific antibodies named as TDP-43-Oligo01 and TDP-43-Oligo02 were used to assess TDP-43O species in the nuclei and cytoplasm of HEK-293 cells. In the nuclear fraction, there was no significant change in HMW TDP-43 species (Figure 2A and 2B), but a significant increase was seen in the cytoplasmic fraction (Figure 2B and 2D). Interestingly, the molecular weights of cytoplasmic TDP-43O were as high as 250 kDa in the cytoplasm of TauO-treated cells. This was a notable contrast to nuclear TDP-43O, which ranged between 50 and 150 kDa. We observed a comparable increase in aggregation from low molecular weight (LMW) species (150 kDa) into HMW TDP-43 (>250 kDa) in the nuclear fractions of rTauO-treated cells (Figure 2C). This mainly occurred in the nuclear fraction probed with the TDP-43-Oligo01 antibody, but a similar increase was also seen in the cytoplasmic fraction using the TDP-43-Oligo02 antibody. A common feature between the antibodies is that they poorly recognize the mTDP-43 in both cellular compartments. TDP-43 Oligo01 and Oligo02 recognized a 36-kDa band in the cytoplasmic fraction, which could be a cleaved TDP-43 fragment. Densitometry analysis of individual bands (75, 150 and above 250 kDa) of cytoplasmic and nuclear fractions of HEK-293 cells probed with both TDP-43 Oligo01 and TDP-43 Oligo02 are presented in Supplementary Figure 2F, G. Overlapped IF signals of TDP-43 Oligo01 and Oligo02 (green) with commercial TDP-43 Ab (red) in HEK-293 treated with exogenous TauO, IF IB are shown in Figure 3E. We also performed IF using TDP-43 Oligo01 (Figure 3F) and Oligo02 (Figure 3G) in HEK-293 exogenously treated with labeled TauO-AF568. The results showed that TauO led to an increase of co-localizing Tau/TDP-43 oligomers as dense aggregates (white arrows).

High levels of WT and P301L Tau differentially modulate TDP-43 in cellular compartments.

We tested TDP-43 oligomeric antibodies in two inducible tau cell models of HEK cells (iHEK). These two cell lines express human WT and P301L mutant tau (WT tau iHEK and P301L iHEK, respectively). Following 24-h Tet treatment, cells expressed high levels of tau compared to untreated cells (−Tet) (Figure 3A–L). We used TDP-43 oligomer antibodies to

investigate cytoplasmic and nuclear TDP-43 levels in WT and P301L tau iHEK cells. We detected large quantities of TDP-43O forms in both compartments of both cell lines compared to untreated cells. Moreover, we observed different band patterns in the cytoplasmic and nuclear fractions. Specifically, the level of TDP-43O probed with TDP-43 Oligo01 decreased in the nuclear and cytoplasmic fractions of WT tau iHEK (Figure 3A–C). We did not observe any compartmental difference in P301L tau iHEK cells (Figure 3D–F). However, different TDP-43 expression patterns were found between the P301L tau and WT tau-expressing iHEK cells when the TDP-43-Oligo02 antibody was used (Figure 3G). There was a significant increase of HMW TDP-43 in the cytoplasm and a decrease in the nuclei of WT tau cells (Figure 3H, I). In P301L tau iHEK, we did not observe any significant cytoplasmic accumulation of TDP-43 in cells probed with TDP-43-Oligo02 (Figure 3J, K). However, a significant reduction of HMW TDP-43 species in the WT tau nuclei was detected (Figure 3L).

In both untreated iHEK cell lines (WT and P301L tau), TDP-43 oligomer antibodies detected several species in the cytoplasmic and nuclear fractions. Recently, cross-linking experiments have revealed that in the normal human brain, TDP-43 exist as dimers and also as a large spectrum of oligomeric species including trimers and tetramers (Afroz et al., 2017). It was previously reported that TDP-43 forms dimers in HEK-293 cells (Shiina et al., 2010). This oligomerization is thought to affect TDP-43's functional roles in RNA binding, probably by its increased affinity and specificity for its RNA targets, and/or via optimal recruitment of other RNA splicing factors. Furthermore, Afroz and colleagues (Afroz et al., 2017) observed that most multimeric TDP-43 species were localized in the nuclei, which is similar to what we observed in IBs with TDP-43 Oligo01 (Figure 3A, D). Therefore, the detection of multimeric TDP-43 in untreated iHEK cells is not surprising. IB with a commercial TDP-43 Ab in WT tau iHEK (−Tet vs +Tet) (Figure 3M) revealed a non-significant reduction of monomeric TDP-43 in the cytoplasm (Figure 3N) and a significant decrement of monomeric TDP-43 in the nuclei (Figure 3O) that was also observed in P301L tau iHEK nuclear fractions (Figure 3P, Q).

The expression of the *MAPT* gene and tau protein in these cell lines was validated by RT-qPCR and IB analysis with Pan-Tau Ab (Tau13); the results showed high expression after Tet incubation (Supplemental Figure 1E–I). Furthermore, IB and RT-qPCR were performed to evaluate TDP-43 protein levels and *TARDBP* gene expression, respectively. There were no significant changes in *TARDBP* gene expression in HEK-293, WT tau and P301L tau iHEK cells (Figure 3R–T). These results suggest that the increase of TDP-43O forms was mainly due to an effect of TauO on the TDP-43 oligomerization process. On the other hand, tau oligomer formation after 24-h induction of HEK cells has been reported (Montalbano et al., 2019), supporting our hypothesis that TDP-43 oligomerization is facilitated by endogenous TauO.

TDP-43O species in AD, ALS and FTD brains.

We IP'ed TDP-43 aggregates from the PBS-soluble fractions of AD, ALS, and FTD brain homogenates using a TDP-43 oligomer-specific antibody. The IP'ed TDP-43 aggregates (F1) along with the PBS-insoluble fraction and input were assessed by filter trap and dot blot

assays using a pTDP-43 antibody (Figure 4A, B). We detected phosphorylated species in the PBS-insoluble fraction and input, but no signal was detected in the IP'ed TDP-43 samples. To validate the presence of TDP-43Os in the brain-derived fractions, we performed IBs with the same antibody used to IP and observed oligomeric TDP-43 in the IP'ed fractions from all three disease states (Figure 4C). The positive signals for TDP-43O observed in the IP'ed fractions was confirmed by dot blot (Figure 4D). The purity of BDT43Os was confirmed by filter Trap assay and dot blot using anti-rabbit and anti-mouse IgG secondary antibodies alone (Supplementary Figure 5A, B). The oligomeric nature of the BDT43Os was confirmed by AFM imaging showing the spherical morphology of the oligomers (Figure 4E). To test whether the BDT43Os (AD, ALS, and FTD) could trigger tau aggregation *in vitro* acting as a templating agent, we cross-seeded recombinant tau monomers (2N4R) with BDT43Os and observed tau oligomer formation by IB with Tau 13 and Tau 5 antibodies (Figure 4F). To clarify the aggregation state and hydrophobicity of BDT43Os cross-seeded TauO, ThT and bis-ANS fluorescence binding assays were performed along with recombinant TauO, TauM, and TauF as controls. Hydrophobic BDT43Os cross-seeded TauO showed a lower binding affinity for ThT as compared to TauF, which served as the positive control (Figure 4G). Bis-ANS spectroscopic analyses showed that BDT43Os cross-seeded TauO and rTauO strongly bound to bis-ANS compared to TauF and TauM (Figure 4H). The oligomeric nature of the BDT43Os cross-seeded TauO was confirmed by AFM imaging showing the spherical morphology of the oligomers (Figure 4I). To further test if seeded tau oligomers form different polymorphs, we treated the three preparations of BDT43O cross-seeded tau oligomers with 0, 1, or 2 μg/mL PK enzyme. IB analysis of cross-seeded tau monomers with BDT43Os showed HMW aggregates using the Tau 5 antibody. As expected, we did not observe any fragmentation in samples without PK enzyme (Figure 4J). At 1 and 2.0 μg/mL PK concentrations, there was not much difference in the cleavage patterns of tau oligomers cross-seeded with BDT43Os and tau oligomers alone (Figure 4K). Recombinant tau monomers and oligomers were used as controls.

TDP-43Os co-localize with beta-amyloid aggregates in AD brain.

Previously we reported that oligomeric TDP-43 co-localizes with Aβ and other proteins in the AD brain (Guerrero-Muñoz et al., 2014). To test co-localization in human AD brains, we performed co-immunofluorescence using the A11 antibody (Kayed et al., 2003) that recognizes oligomeric structures in combination with both TDP-43O-specific antibodies and others that recognize ß-amyloid (6E10), amyloid plaques (OC), Tau13. For each antibody combination with A11, we evaluated co-localization grade by calculating the PCC. We observed very strong co-localization between A11 and OC (PCC>0.8), TDP-43-Oligo01 (PCC>0.8), and TDP-43-Oligo02 (PCC>0.8) antibodies (Figure 5B, D, and E), indicating the presence of TDP-43 oligomeric structures. A positive overlap ($0.6<PCC<0.8$) was observed between A11 with 6E10 and Tau13 (Figure 5A and C, respectively) indicating intermediate co-localization. The PCC graph summarizes and compares co-localization of A11 with each of the other five antibodies (6E10, OC, Tau13, TDP-43-Oligo01, and TDP-43-Oligo02) and the internal variation between ROIS (10 per image, Figure 5F). Immunostaining of control brain sections for A11, TDP-43, pTDP43 with TDP-43 Oligo01 is shown in Supplemental Figure 5C.

We studied TDP-43 oligomer patterns in AD, ALS, and FTD brain tissues by performing IF using the TDP-43-Oligo01 Ab with commercial TDP-43 and pTDP-43 Abs (Figure 6A–C). Differential distributions of oligomeric TDP-43 were found among the diseases. In particular, AD and ALS showed marked TDP-43O deposition with more diffuse signals in the AD brains. However, in FTD we observed a spotty distribution of TDP-43-Oligo01-positive aggregates. Co-staining of TDP-43Os with Tau13 and Tau Oligomeric Monoclonal Ab (TOMA-2) (Montalbano et al., 2020b) revealed limited co-localization coefficients in AD brain tissue (Figure 6D and E, PCC: 0.2–0.3). However, we observed different patterns in the co-localization maps of TDP-43Os and TOMA-2 staining. TDP-43 Oligo01/TOMA-2 showed a more diffuse signal, while TDP-43 Oligo02/TOMA-2 had a spotty (aggregated) distribution. These observations indicate that the patterns of oligomeric TDP-43 and tau deposition in these neurodegenerative diseases are heterogeneous. High-magnification images of AD brain sections co-stained with TOMA2/TDP-43-Oligo01 confirmed extranuclear TDP-43 deposition and its limited co-localization with tau oligomers (Figure 6F).

Discussion

Phosphorylated and cleaved forms of TDP-43 are components of characteristic proteinaceous inclusions that are mainly found in ALS and FTD (Ling et al., 2013). Intracellular accumulation of this RBP has also been observed in other dementias including AD (Chang et al., 2016) and dementia with Lewy bodies (DLB) in concurrence with tau and α-synuclein aggregation (Higashi et al., 2007; McAleese et al., 2017). However, the significance of TDP-43 pathology in AD and DLB is unknown due to the ambiguity surrounding its biochemical features, especially regarding its oligomeric forms. To determine whether tau and TDP-43 co-exist as oligomeric forms, we performed a series of immunohistochemical and biochemical analyses of AD, ALS, and FTD brain tissue using a newly developed set of antibodies that specifically recognize TDP-43 oligomers.

We observed that Exo-TauO modulates monomeric TDP-43 compartmentalization in HEK-293 cells, regardless of TDP-43 phosphorylation state. In particular, TauO seem to increase the nuclear levels of both phosphorylated and non-phosphorylated TDP-43 monomers. This was evaluated using two commercial antibodies for TDP-43.

Using the newly developed TDP-43-Oligo (01 and 02) antibodies, we observed a shift from LMW to HMW TDP-43 forms after Exo-TauO treatment. We did not observe statistically significant differences in TDP-43 protein levels in the cytoplasmic or nuclear fractions. This suggests that TauO mediates the shift of TDP-43 from LMW to HMW in both cellular compartments, and they also increase nuclear levels of monomeric TDP-43. The presence of TDP-43 oligomers in AD, ALS, and FTD was evaluated by immunoprecipitating TDP-43 aggregates and assessing them by filter trap and dot blot assays, as well as in IF experiments.

We evaluated the co-localization scores for TDP-43 oligomers and other oligomeric proteins (amyloid, tau) using the anti-oligomeric A11 antibody. We observed a strong association of TDP-43 oligomeric structures (positive for A11, TDP-43-Oligo01, and Oligo02) with amyloid-plaques (OC), β-amyloid (6E10), and tau (Tau13).

These results suggested co-accumulation of TDP-43 with β-amyloid and tau, confirming a previous report (Higashi et al., 2007). Furthermore, we also noted different HMW TDP-43 aggregates in the nuclei and cytoplasm of WT and P301L tau iHEK cells, indicating that different oligomeric forms co-exist intracellularly but with compartment-dependent profiles. Commercial and in-house antibodies have supported these findings based on IB analyses with cell fractions from WT and P301L tau iHEK cells.

In vitro tau aggregation can be stimulated by widely used inducers including arachidonic acid, heparin sulfate, alkyl sulfate, polyphosphates that mimic cellular polyanions, and lipid vesicles (Chirita et al., 2003; Cremers et al., 2016; Mutreja and Gamblin, 2017). In addition, tau aggregation can be triggered by templating agents like recombinant oligomeric species of other amyloidogenic proteins such as Aβ and α-synuclein (Castillo-Carranza et al., 2018; Sengupta et al., 2020), as well as brain-derived oligomeric assemblies from AD and other tauopathies (Gerson et al., 2014; Lasagna-Reeves et al., 2012). All these preparations may lead to the formation of unique conformations that may have different seeding capacities and structures. We investigated the cross-seeding capacities of TDP-43Os immunoprecipitated from AD, ALS, and FTD brains inducing oligomerization of tau monomers; our results suggest that TDP-43 can be used as templating agent to trigger tau aggregation *in vitro*. However, the PK digestion assay experiments did not show relevant differences in the proteolytic patterns of BDT43Os cross-seeded with tau monomers.

The implications of these findings are considerable, and they advance our knowledge in the pathogeneses and propagation of several proteinopathies. Collectively, our results suggest that TDP-43 has distinctive oligomeric forms specific to their intracellular localization, and they can be formed in the brains of AD and FTD cases but are rare in ALS. We and others have described the association of TDP-43 with Aβ, and few studies have noted that TDP-43 and tau interact. However, the specific description of TDP-43Os associating with tau is an exciting and novel finding.

Whether the concurrence of ALS/FTD TDP-43 and AD-tau is incidental is still controversial because aging is the major risk factor for all three diseases. The histopathological hallmarks of these conditions are quite different, but it is becoming evident that TDP-43 accumulation occurs in AD (Tremblay et al., 2011) and could also lead to abnormal tau expression (Gu et al., 2017; Gu et al., 2019). Further elucidation of the co-existence of TDP-43, tau, and other proteins in aggregates in the brains of patients with ALS/FTLD will be useful for understanding how these proteins influence disease development and clinical manifestations. However, the fact that TDP-43Os associate with other amyloidogenic proteins (Aβ and tau) indicates that TDP-43 oligomers have varying affinities for amyloid plaques and tau aggregates, suggesting co-partnerships in the pathogeneses of these neurodegenerative diseases.

Many other RBPs involved in dysregulation event abnormally accumulate in different cell compartments, creating an ideal environment for toxic oligomeric species deposition. Future investigations will elucidate the nature of the association between TDP-43 with tau. We will further explore whether this association is pathogenic and if it occurs in a liquid phase-dependent manner (Elbaum-Garfinkle, 2019). Further studies will be necessary to clarify the

mechanism underlying the toxic interplay between TDP-43 and tau. Here we speculated on potential interactions and accumulation in cell models and diseased human brains. It will be crucial to further characterize TDP-43O structure and function to better address the physiological and pathological effects of this species.

Supplementary Material

Refer to Web version on PubMed Central for supplementary material.

Acknowledgments and Funding

We thank the members of the Kayed lab for their support and help, Nicha Puangmalai, PhD for HEK-293 cell cultures and Jai Rudra, PhD (Washington University in St. Louis) for the synthesis of the three TDP-43 peptides. We thank Kathleen Farmer, Omar D. Johnson, Cynthia A. Duarte, and Eric A. Heidelman for editing and proofreading the manuscript. The final version was edited by Lindsay Reese, Ph.D. (SciReviser). This work was supported by grants from The National Institute of Health AG054025, NS094557, AG055771 and R01AG060718 (R.K.), The Gillson Longenbaugh Foundation and the Mitchell Center for Neurodegenerative Disease.

Abbreviations:

AD	Alzheimer’s disease
ALS	amyotrophic lateral sclerosis
BDT43Os	brain-derived TDP-43 oligomers
FTD	frontotemporal dementia
HMW	high molecular weight
iHEK	inducible human embryonic kidney cells
LMW	low molecular weight
MAPT	Microtubule-Associated Protein Tau
mTDP-43	monomeric TDP-43
RBPs RNA	binding proteins
TARDBP	transactive response (TAR)-DNA binding protein
TauF	tau fibrils
TauM	tau monomers
TauO	tau oligomers
TDP-43 TAR	DNA binding protein-43
TDP-43Os	TDP-43 oligomers

References

Afroz T, et al., 2017 Functional and dynamic polymerization of the ALS-linked protein TDP-43 antagonizes its pathologic aggregation. Nature Communications. 8, 45.

Berning BA, Walker AK, 2019 The Pathobiology of TDP-43 C-Terminal Fragments in ALS and FTLD. Frontiers in Neuroscience. 13.

Bittar A, et al., 2019 Neurotoxic tau oligomers after single versus repetitive mild traumatic brain injury. Brain communications. 1, fcz004–fcz004. [PubMed: 31608324]

Butti Z, Patten SA, 2019 RNA Dysregulation in Amyotrophic Lateral Sclerosis. Frontiers in Genetics. 9.

Castillo-Carranza DL, et al., 2018 α-Synuclein Oligomers Induce a Unique Toxic Tau Strain. Biol Psychiatry. 84, 499–508. [PubMed: 29478699]

Chang XL, et al., 2016 The Role of TDP-43 in Alzheimer's Disease. Mol Neurobiol. 53, 3349–3359. [PubMed: 26081142]

Chen Y, Cohen TJ, 2019 Aggregation of the nucleic acid-binding protein TDP-43 occurs via distinct routes that are coordinated with stress granule formation. J Biol Chem. 294, 3696–3706. [PubMed: 30630951]

Chirita CN, et al., 2003 Anionic micelles and vesicles induce tau fibrillization in vitro. J Biol Chem. 278, 25644–50. [PubMed: 12730214]

Choksi DK, et al., 2014 TDP-43 Phosphorylation by casein kinase Iepsilon promotes oligomerization and enhances toxicity in vivo. Hum Mol Genet. 23, 1025–35. [PubMed: 24105464]

Chornenkyy Y, et al., 2019 Tau and TDP-43 proteinopathies: kindred pathologic cascades and genetic pleiotropy. Lab Invest. 99, 993–1007. [PubMed: 30742063]

Chou C-C, et al., 2018 TDP-43 pathology disrupts nuclear pore complexes and nucleocytoplasmic transport in ALS/FTD. Nature Neuroscience. 21, 228–239. [PubMed: 29311743]

Cremers CM, et al., 2016 Polyphosphate: A Conserved Modifier of Amyloidogenic Processes. Mol Cell. 63, 768–80. [PubMed: 27570072]

Ederle H, Dormann D, 2017 TDP-43 and FUS en route from the nucleus to the cytoplasm. FEBS Lett. 591, 1489–1507. [PubMed: 28380257]

Elbaum-Garfinkle S, 2019 Matter over mind: Liquid phase separation and neurodegeneration. J Biol Chem. 294, 7160–7168. [PubMed: 30914480]

Ferrari R, et al., 2011 FTD and ALS: a tale of two diseases. Curr Alzheimer Res. 8, 273–94. [PubMed: 21222600]

Gao J, et al., 2018 Pathomechanisms of TDP-43 in neurodegeneration. Journal of neurochemistry. 10.1111/jnc.14327.

Gasset-Rosa F, et al., 2019 Cytoplasmic TDP-43 De-mixing Independent of Stress Granules Drives Inhibition of Nuclear Import, Loss of Nuclear TDP-43, and Cell Death. Neuron. 102, 339–357 e7. [PubMed: 30853299]

Gerson JE, et al., 2017 Tau Oligomers as Pathogenic Seeds: Preparation and Propagation In Vitro and In Vivo. Methods Mol Biol. 1523, 141–157. [PubMed: 27975249]

Gerson JE, et al., 2014 Characterization of tau oligomeric seeds in progressive supranuclear palsy. Acta neuropathologica communications. 2, 73–73. [PubMed: 24927818]

Ghag G, et al., 2018 Soluble tau aggregates, not large fibrils, are the toxic species that display seeding and cross-seeding behavior. Protein Sci. 27, 1901–1909. [PubMed: 30125425]

Gu J, et al., 2017 Transactive response DNA-binding protein 43 (TDP-43) regulates alternative splicing of tau exon 10: Implications for the pathogenesis of tauopathies. The Journal of biological chemistry. 292, 10600–10612. [PubMed: 28487370]

Gu J, et al., 2019 Cyclic AMP-Dependent Protein Kinase Phosphorylates TDP-43 and Modulates Its Function in Tau mRNA Processing. Journal of Alzheimer's disease : JAD. 70, 1093–1102.

Guenther EL, et al., 2018 Atomic structures of TDP-43 LCD segments and insights into reversible or pathogenic aggregation. Nat Struct Mol Biol. 25, 463–471. [PubMed: 29786080]

Guerrero-Muñoz MJ, et al., 2014 Amyloid-β oligomers as a template for secondary amyloidosis in Alzheimer's disease. Neurobiol Dis. 71, 14–23. [PubMed: 25134727]

Hedl TJ, et al., 2019 Proteomics Approaches for Biomarker and Drug Target Discovery in ALS and FTD. Frontiers in Neuroscience. 13.

Higashi S, et al., 2007 Concurrence of TDP-43, tau and alpha-synuclein pathology in brains of Alzheimer's disease and dementia with Lewy bodies. Brain Res. 1184, 284–94. [PubMed: 17963732]

Johnson BS, et al., 2009 TDP-43 is intrinsically aggregation-prone, and amyotrophic lateral sclerosis-linked mutations accelerate aggregation and increase toxicity. J Biol Chem. 284, 20329–39. [PubMed: 19465477]

Kayed R, et al., 2003 Common structure of soluble amyloid oligomers implies common mechanism of pathogenesis. Science. 300, 486–9. [PubMed: 12702875]

Lasagna-Reeves CA, et al., 2012 Identification of oligomers at early stages of tau aggregation in Alzheimer's disease. FASEB J. 26, 1946–59. [PubMed: 22253473]

Ling SC, et al., 2013 Converging mechanisms in ALS and FTD: disrupted RNA and protein homeostasis. Neuron. 79, 416–38. [PubMed: 23931993]

Lo Cascio F, et al., 2020. Modulating Disease-Relevant Tau Oligomeric Strains by Small Molecules. J Biol Chem.

Lo Cascio F, Kayed R, 2018a Azure C Targets and Modulates Toxic Tau Oligomers. ACS Chem Neurosci. 9, 1317–1326. [PubMed: 29378132]

Lo Cascio F, Kayed R, 2018b Azure C Targets and Modulates Toxic Tau Oligomers. 9, 1317–1326.

Lo Cascio F, et al., 2019 Toxic Tau Oligomers Modulated by Novel Curcumin Derivatives. Sci Rep. 9, 19011. [PubMed: 31831807]

Mandrioli J, et al., 2020 ALS and FTD: Where RNA metabolism meets protein quality control. Semin Cell Dev Biol. 99, 183–192. [PubMed: 31254610]

Margittai M, Langen R, 2004 Template-assisted filament growth by parallel stacking of tau. Proc Natl Acad Sci U S A. 101, 10278–83. [PubMed: 15240881]

Margittai M, Langen R, 2006 Side chain-dependent stacking modulates tau filament structure. J Biol Chem. 281, 37820–7. [PubMed: 17023423]

McAleese KE, et al., 2017 TDP-43 pathology in Alzheimer's disease, dementia with Lewy bodies and ageing. Brain Pathol. 27, 472–479. [PubMed: 27495267]

Monahan Z, et al., 2016 Stress granules at the intersection of autophagy and ALS. Brain Res. 1649, 189–200. [PubMed: 27181519]

Montalbano M, et al., 2020a RNA-binding proteins Musashi and tau soluble aggregates initiate nuclear dysfunction. Nat Commun. 11, 4305. [PubMed: 32855391]

Montalbano M, et al., 2020b RNA-binding proteins Musashi and tau soluble aggregates initiate nuclear dysfunction. Nature Communications. 11, 4305.

Montalbano M, et al., 2019 Tau oligomers mediate aggregation of RNA-binding proteins Musashi1 and Musashi2 inducing Lamin alteration. Aging Cell. 18, e13035. [PubMed: 31532069]

Mutreja Y, Gamblin TC, 2017 Optimization of in vitro conditions to study the arachidonic acid induction of 4R isoforms of the microtubule-associated protein tau. Methods Cell Biol. 141, 65–88. [PubMed: 28882312]

Neumann M, et al., 2006 Ubiquitinated TDP-43 in frontotemporal lobar degeneration and amyotrophic lateral sclerosis. Science. 314, 130–3. [PubMed: 17023659]

Nussbacher JK, et al., 2015 RNA-binding proteins in neurodegeneration: Seq and you shall receive. Trends in neurosciences. 38, 226–236. [PubMed: 25765321]

Nussbacher JK, et al., 2019 Disruption of RNA Metabolism in Neurological Diseases and Emerging Therapeutic Interventions. Neuron. 102, 294–320. [PubMed: 30998900]

Prasad A, et al., 2019 Molecular Mechanisms of TDP-43 Misfolding and Pathology in Amyotrophic Lateral Sclerosis. Frontiers in Molecular Neuroscience. 12.

Puangmalai N, et al., 2020 Internalization mechanisms of brain-derived tau oligomers from patients with Alzheimer's disease, progressive supranuclear palsy and dementia with Lewy bodies. Cell Death Dis. 11, 314. [PubMed: 32366836]

Ratti A, Buratti E, 2016 Physiological functions and pathobiology of TDP-43 and FUS/TLS proteins. J Neurochem. 138 Suppl 1, 95–111. [PubMed: 27015757]

Sengupta U, et al., 2018a Preparation and Characterization of Tau Oligomer Strains. Methods in molecular biology (Clifton, N.J.). 1779, 113–146.

Sengupta U, et al., 2018b Formation of Toxic Oligomeric Assemblies of RNA-binding Protein: Musashi in Alzheimer's disease. Acta Neuropathologica Communications. 6, 113. [PubMed: 30367664]

Sengupta U, et al., 2020 Polymorphic α-Synuclein Strains Modified by Dopamine and Docosahexaenoic Acid Interact Differentially with Tau Protein. Molecular Neurobiology.

Shiina Y, et al., 2010 TDP-43 dimerizes in human cells in culture. Cell Mol Neurobiol. 30, 641–52. [PubMed: 20043239]

Takeda T, 2018 Possible concurrence of TDP-43, tau and other proteins in amyotrophic lateral sclerosis/frontotemporal lobar degeneration. Neuropathology. 38, 72–81. [PubMed: 28960544]

Tremblay C, et al., 2011 Accumulation of transactive response DNA binding protein 43 in mild cognitive impairment and Alzheimer disease. J Neuropathol Exp Neurol. 70, 788–98. [PubMed: 21865887]

Highlights

- TDP-43 oligomers occur in AD, ALS and FTD pathologies
- Tau modulates TDP-43 cellular localization and oligomerization
- Brain-derived TDP-43 oligomers can act as seeds for tau oligomerization in vitro

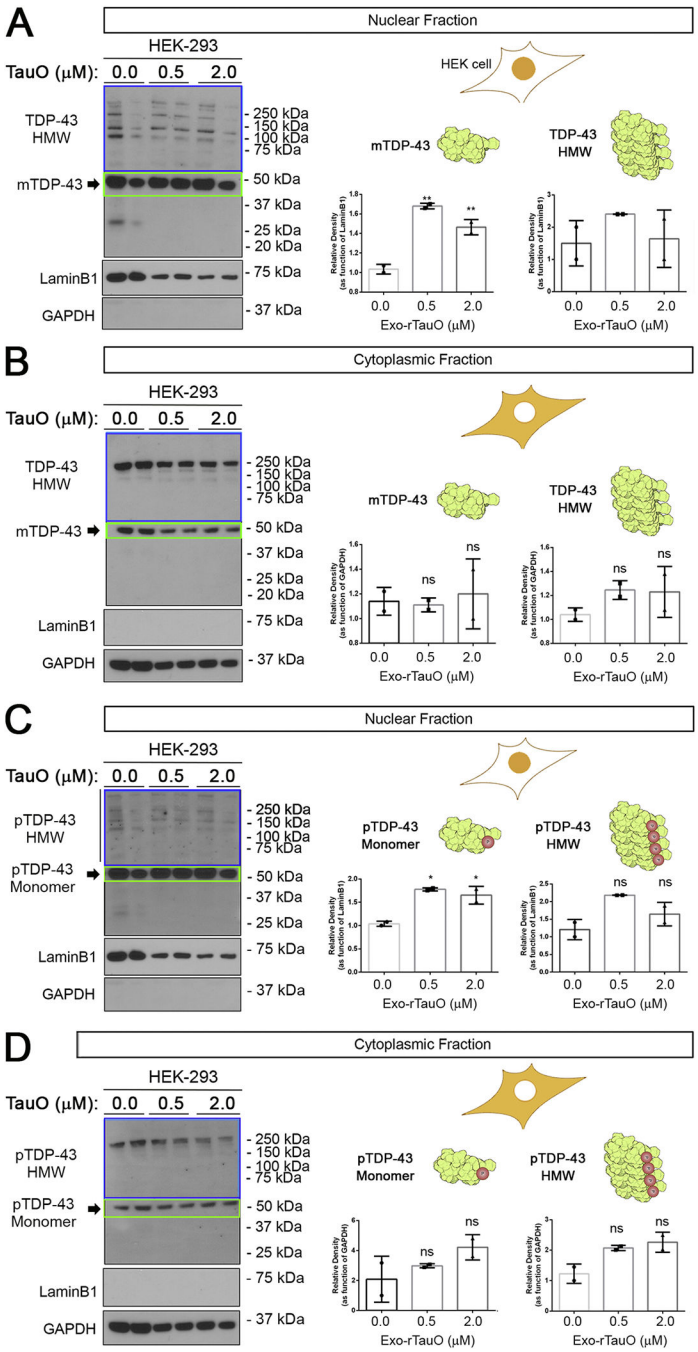

Figure 1. Exo-rTauO alter TDP-43 localization in HEK-293 cells.

(A) IB of HEK-293 nuclear fractions incubated with rTauO (0.5 and 2.0 μM), probed with a commercial TDP-43 antibody (Ab109535). Significant increases of monomeric TDP-43 were observed in 0.5 and 2.0 μM treated cells (F: 69.59, P value: 0.0031, $^{**}p<0.05$ R square: 0.9789), with no significant difference in HMW TDP-43 (P value: 0.4394). **(B)** IB of TDP-43 cytoplasmic fractions of HEK-293 cells incubated with rTauO (0.5 and 2.0μM) did not show significant differences in cytoplasmic TDP-43 levels (TDP-43 monomer P value: 0.8818, TDP-43 HMW P value: 0.3636). **(C)** IB of pTDP-43 nuclear fractions of HEK-293

incubated with rTauO (0.5 and 2.0 μM) showing a significant increase (F: 22.73, P value: 0.0154, *p<0.05, R square: 0.9381) of monomeric pTDP-43 with no significant HMW pTDP-43 (P value: 0.0702). **(D)** IB of pTDP-43 cytoplasmic fractions of HEK-293 incubated with rTauO (0.5 and 2.0 μM). No significant differences was observed for monomeric (P value: 0.2570) or HMW pTDP-43 (P value: 0.0585). Monomer (green box) and HMW (blue box) TDP-43 are quantified and presented in separate bar graphs (Mean ±SD). LaminB1 and GAPDH were used as loading controls for the nuclear and cytoplasmic fractions, respectively. Ordinary one-way ANOVA with Dunnett's multiple comparison test was performed among the three groups in three independent experiments. The HEK-293 schematic cell is represented with the nuclei or cytoplasm in orange to indicate the analyzed compartment. mTDP-43 and HMW TDP-43 are represented by a rendered NMR structure of RNA-Motif domains of TDP-43 (Uniprot Number: 4BS2). Drawings and protein renderings were produced with Bio Render Software.

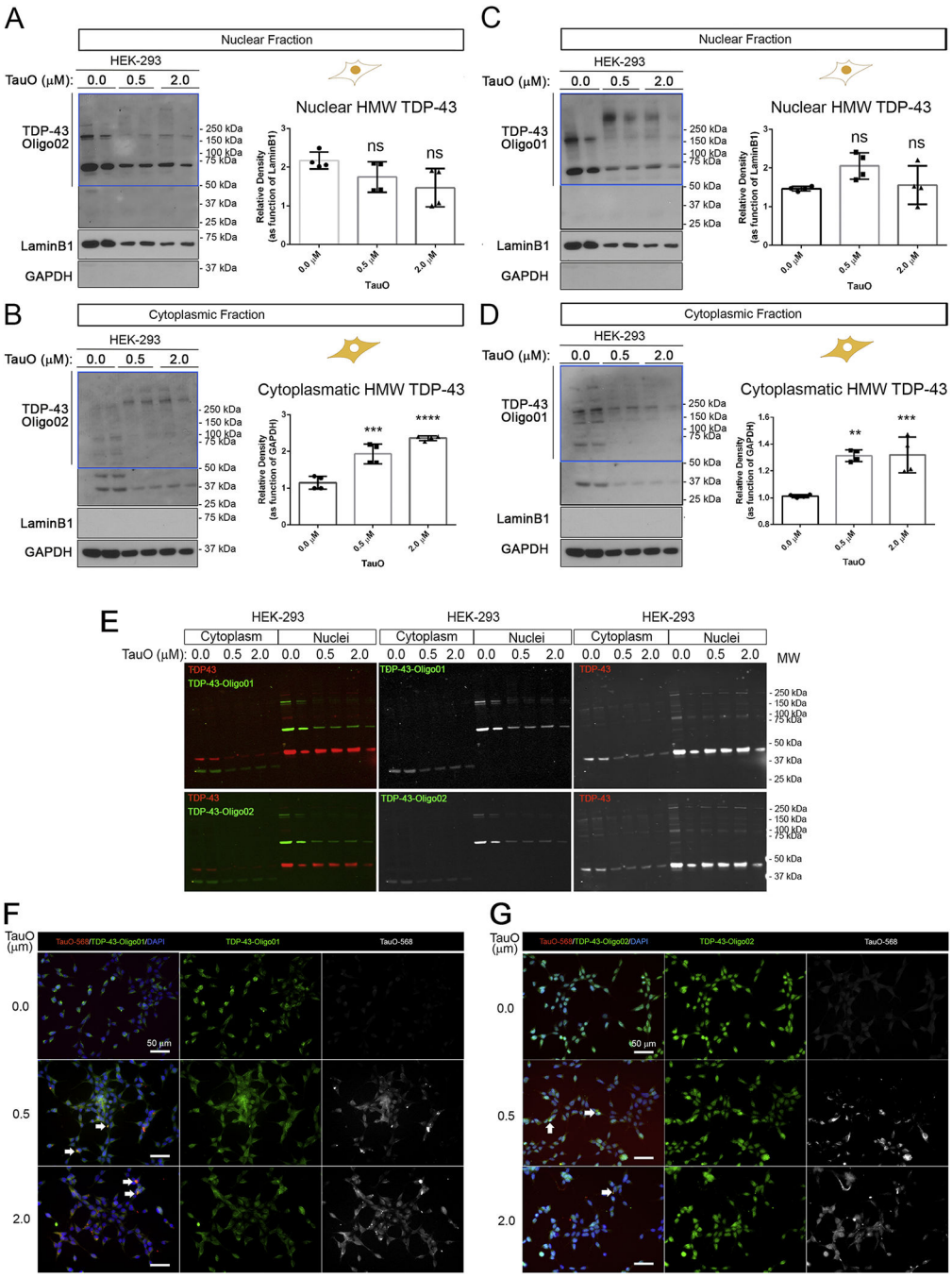

Figure 2. Exo-rTauO induce cytoplasmic TDP-43O accumulation.

(A) IB of nuclear fractions from HEK-293 untreated and treated with TauO 0.5 and 2.0 μM probed with TDP-43-Oligo02 antibody. Relative densitometry of HMW (blue box) is represented (P value: 0.0806). **(B)** IB of cytoplasmic fractions from HEK-293 untreated and incubated with TauO (0.5 and 2.0 μM) probed with TDP-43-Oligo02 antibody. Relative densitometry of HMW (blue box) is presented (F: 42.74, P value: <0.0001, R square: 0.9047). **(C)** IB of nuclear fractions from HEK-293 cells untreated and treated with TauO (0.5 and 2.0 μM) with TDP-43-Oligo01 antibody. Relative densitometry of HMW TDP-43

(blue box) is represented (P value: 0.0866). **(D)** IB of cytoplasmic fractions of HEK-293 cells untreated and treated in with TauO (0.5 and 2.0 μM) with TDP-43-Oligo01 antibody. Relative densitometry of HMW (blue box) is represented (F: 18.50, P value: 0.0006, R square 0.8044). All sections present relative quantification of TDP-43Os and values are presented in separate bar graphs (Mean±SD). LaminB1 and GAPDH have been used as loading control for nuclear and cytoplasmic fractions, respectively. Ordinary one-way ANOVA with Dunnett's multiple comparison test was performed among the three groups in three independent experiments. TDP-43 Oligo01 and TDP-43 Oligo02 immunoblots were conducted in the same membrane. **(E)** Immunofluorescence blots (LI-COR system) of commercial TDP-43 (red) and TDP-43 Oligo01 and Oligo02 (green) Abs in HEK-293 cells treated with TauOs. Colored merge and single gray channels (TDP-43O Abs) are represented. **(F)** Representative IF images of HEK-293 treated with labeled TauO-AF568 (0.5 and 2.0 μM) and stained with TDP-43 Oligo01 (green) and DAPI (nuclei, blue). Magnification: 40x and white scale bar: 50 μm. **(G)**. Representative IF images of HEK-293 treated with labeled TauO-AF568 (0.5 and 2.0 μM) and stained with TDP-43 Oligo02 (green) and DAPI (nuclei, blue). Magnification: 40x and white scale bar: 50 μm. White arrows in F and G indicate overlapping signal for TauO-568 and TDP-43Os.

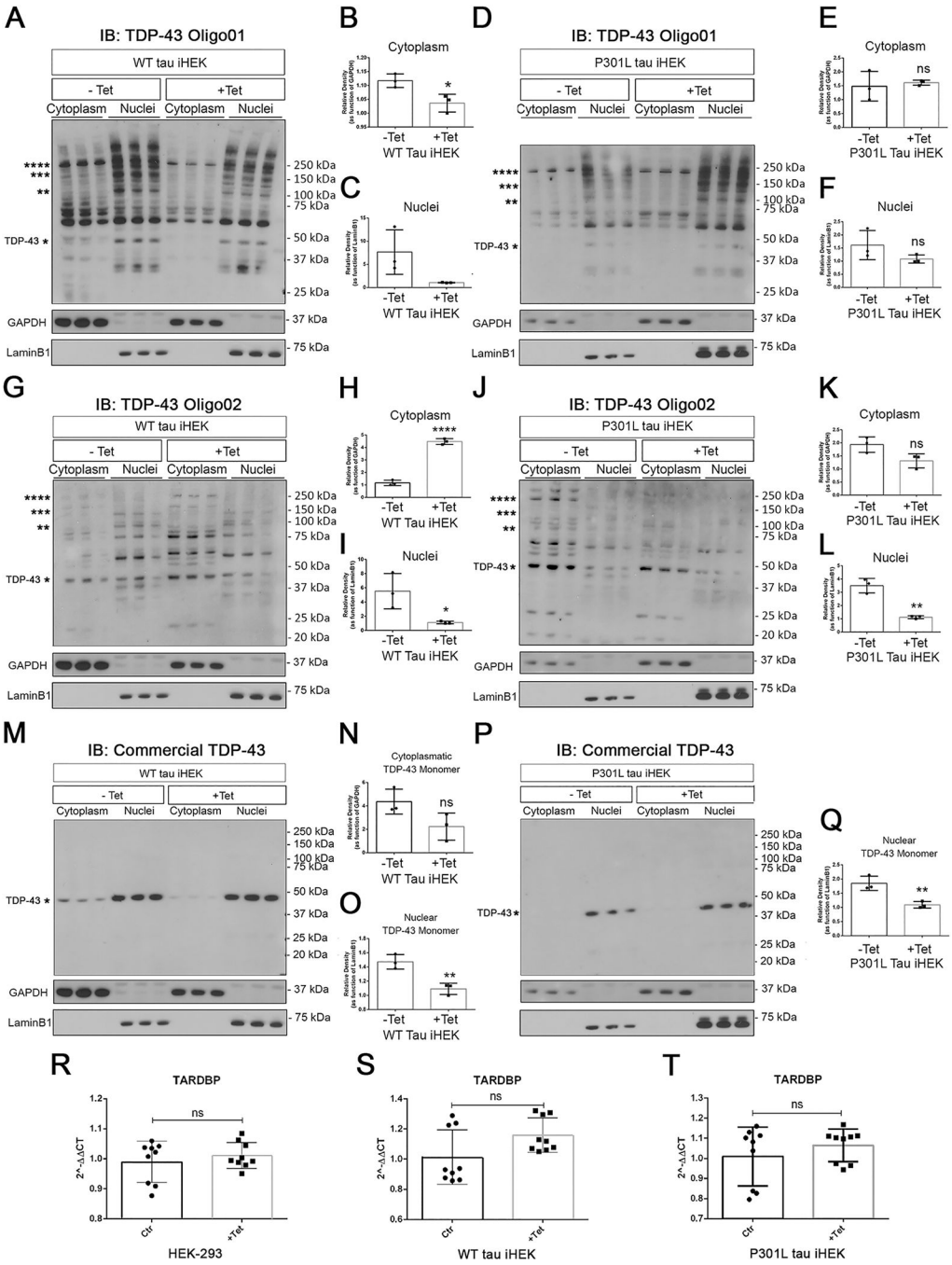

Figure 3. High Tau levels do not modulate *TARDBP* gene expression but regulate TDP-43 oligomerization in iHEK.

(A) IB of TDP-43 Oligo01 in cytoplasmic and nuclear fractions of WT tau iHEK (−Tet and +Tet). **(B)** Relative density of HMW TDP-43 in the cytoplasmic fraction (−Tet vs. +Tet, **p=0.0253*). **(C)** Relative density of HMW of TDP-43 in the nuclear fraction (−Tet vs. +Tet, ns, *p=0.0756*). **(D)** IB of TDP-43 Oigo01 in the cytoplasmic and nuclear fractions of P301L tau iHEK. **(E)** Relative density of HMW TDP-43 in the cytoplasmic fraction (−Tet vs. +Tet, ns, *p=0.7002*) of P301L tau iHEK. **(F)** Relative density of HMW TDP-43 in the nuclear

fraction (ns, *p=0.1863*) of P301L tau iHEK. TDP-43-Oligo01 Ab was used to detect patterns in both compartments before and after Tet incubation. **(G)** IB of TDP-43 Oligo02 in the cytoplasmic and nuclear fractions of WT tau iHEK (−Tet and +Tet). **(H)** Relative density of HMW TDP-43 in the cytoplasmic fraction (−Tet vs. +Tet, ****$p<0.0001$) of WT tau iHEK. **(I)** Relative density of HMW TDP-43 in the nuclear fraction of WT tau iHEK (−Tet vs. +Tet, *$p=0.0375$). **(J)** IB of TDP-43 Oligo02 in the cytoplasmic and nuclear fractions of P301L tau iHEK (−Tet and +Tet). **(K)** Relative density of HMW TDP-43 in the cytoplasmic fraction (−Tet vs. +Tet; ns, $p=0.0542$) of P301L tau iHEK. **(L)** Relative density of HMW TDP-43 in the nuclear fraction of P301L tau iHEK (−Tet vs. +Tet, *$p=0.0018$). **(M)** IB of commercial TDP-43 Ab in the cytoplasmic and nuclear fractions of WT tau iHEK (−Tet and +Tet). **(N)** Relative density of HMW TDP-43 in the cytoplasmic fraction (−Tet vs. +Tet; ns, $p=0.0793$) of WT tau iHEK. **(O)** Relative density of HMW TDP-43 in the nuclear fraction of WT tau iHEK (−Tet vs. +Tet, **$p=0.0069$). **(P)** IB of commercial TDP-43 Ab in the cytoplasmic and nuclear fractions of P301L tau iHEK (−Tet and +Tet). **(Q)** Relative density of HMW TDP-43 in the nuclear fraction (−Tet vs. +Tet, ** $p=0.0093$) of P301L tau iHEK. **(R-T)** RT-qPCR of *TARDBP* expression in HEK-293, WT, and P301L-expressing tau iHEK cells, respectively. Unpaired t-tests were used to compared untreated (−Tet) and treated (+Tet) groups. HEK-293 −Tet vs. +Tet ns, p=0.4520; P301L tau iHEK −Tet vs. +Tet ns, p=0.3377 and WT tau iHEK ns, p=0.0588. The same membrane (for WT and P301L tau iHEK) was immunoblotted for three different Abs (TDP-43 Oligo01, TDP-43 Oligo02, and commercial TDP-43). Each membrane includes three samples per condition. Unpaired t-tests were performed to compare HMW TDP-43 in the cytoplasm and nucleus of −Tet and +Tet iHEK. Values are represented as box-and-whisker plots with bars (Mean±SD).

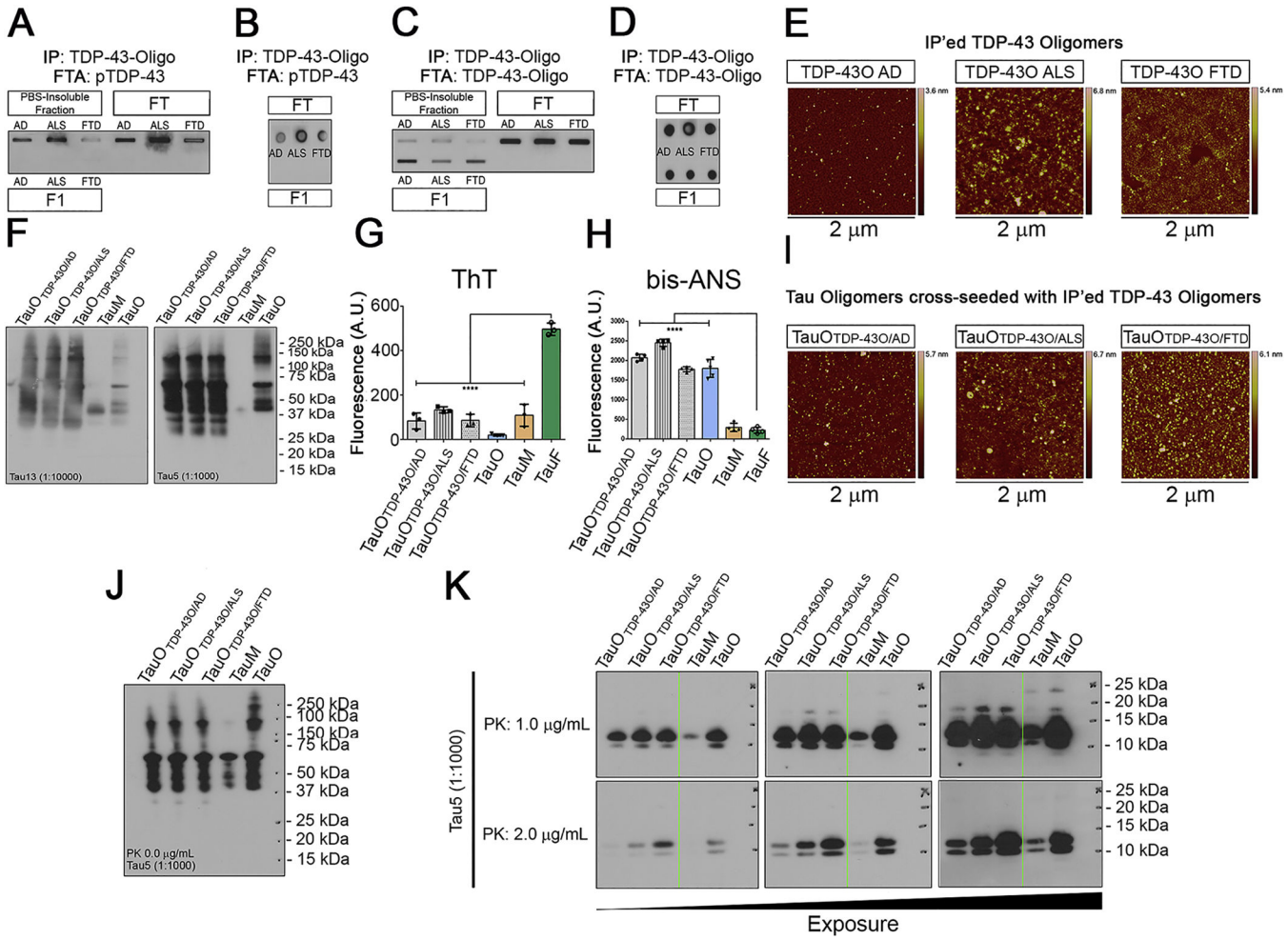

Figure 4. TDP-43O seeding properties.

(A) Filter Trap assay of PBS-insoluble, FT, and IP'ed BDT43Os (F1) and immunoblotted (IB) with the pTDP-43 antibody. **(B)** Dot blot of FT and F1 BDT43Os and IB with the pTDP-43 antibody. **(C)** Filter Trap of PBS-insoluble, FT, and IP'ed BDT43Os (F1) and IB with the TDP-43O antibody **(D)** Dot blot of IP (FT and F1) BDT43O and IB with TDP-43O antibody. **(E)** Representative AFM images of IP'ed BDT43Os from AD, ALS and FTD. **(F)** Tau13 and Tau5 IB of BDT43O (AD, ALS, and FTD) cross-seeded with TauM. TauM and TauO were used as controls (Lanes 4 and 5, respectively). **(G)** Fluorescence intensity measurement of ThT for BDT43Os and controls (TauO, TauM, and TauF). ThT spectroscopic analyses showed that hydrophobic BDT43Os and control TauO and TauM have significantly less binding affinity for ThT than TauF (one-way ANOVA, Dunnett's multiple comparisons test ****p<0.001). **(H)** Fluorescence intensity measurement of bis-ANS to BDT43Os and controls (TauO, TauM, and TauF). Bis-ANS spectroscopic analyses showed that hydrophobic BDT43Os and TauO have significantly higher binding affinity for bis-ANS than TauF and TauM (one-way ANOVA, Dunnett's multiple comparisons test ****p<0.001). **(I)** Representative AFM images of TauO cross-seeded with IP'ed BDT43Os from AD, ALS and FTD. **(J)** Tau5 IB of 0 μg/mL PK BDT43O (AD, ALS, and FTD) cross-seeded with TauM; TauM and TauO were used as controls (Lanes 4 and 5, respectively). **(K)**

Tau5 IB of 1.0 (top) and 2.0 (bottom) μg/mL PK BDT43O (AD, ALS, and FTD) cross-seeded with TauM; TauM and TauO were used as controls (Lanes 4 and 5, respectively). The three immunoblots presented are different exposures of the same immunoblot.

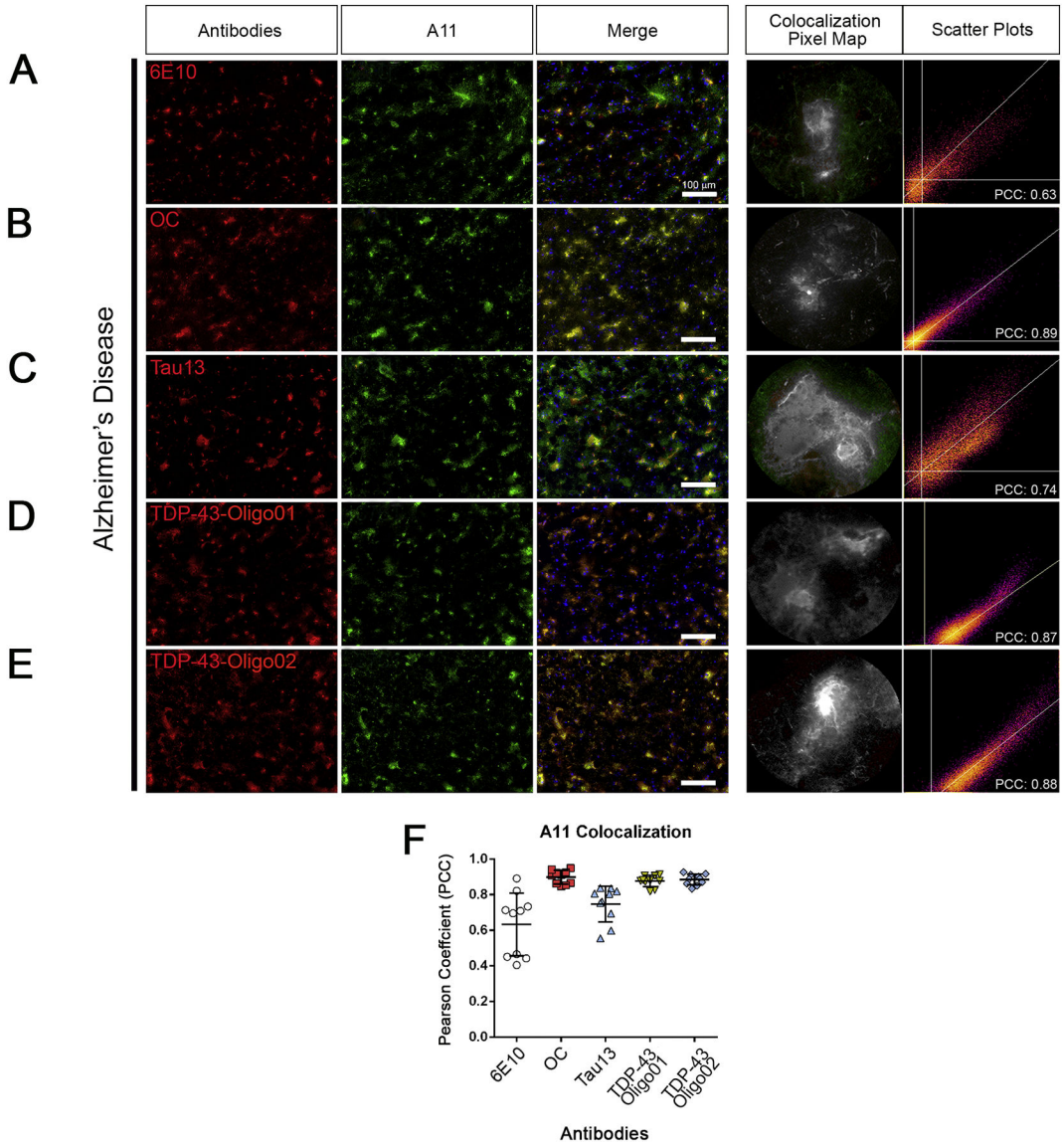

Figure 5. TDP-43Os co-localize with oligomeric Aβ structures in AD brain.

(A) Representative immunofluorescence images of cortical brain tissue sections from patients with AD stained with A11 (green) and 6E10 (red). Merge is presented along with a representative co-localization pixel map and intensity scatter plot. **(B)** IF co-staining with A11 (green) with OC (red). Merge is presented with a representative co-localization pixel map and intensity scatter plot. **(C)** IF co-staining of A11 (green) with Tau13 (red). Merge is presented with a representative co-localization pixel map and intensity scatter plot (*PCC*=0.89). **(D)** IF co-staining with A11 (green) with TDP-43-Oligo01 (red). Merge is presented with a representative co-localization pixel map and intensity scatter plot (*PCC*=0.87). **(E)** IF co-staining of A11 (green) with TDP-43-Oligo02 (red). Merge is presented with a representative co-localization pixel map and intensity scatter plot (*PCC*=0.88). **(F)** Pearson coefficient scatter plot of combined co-staining of A11 with OC, Tau13, TDP-43-Oligo01, andTDP-43-Oligo02 (from left to right). All images were taken

with a 20x objective and represented in green (A11), red (other antibodies) and merge, white scale bar: 100 μm. Representative co-localization (*green+red=grey*) pixel maps represent random ROIs enlarged, and the scatter plot is related to those 10 ROIs (n=3 for each AD case analyzed).

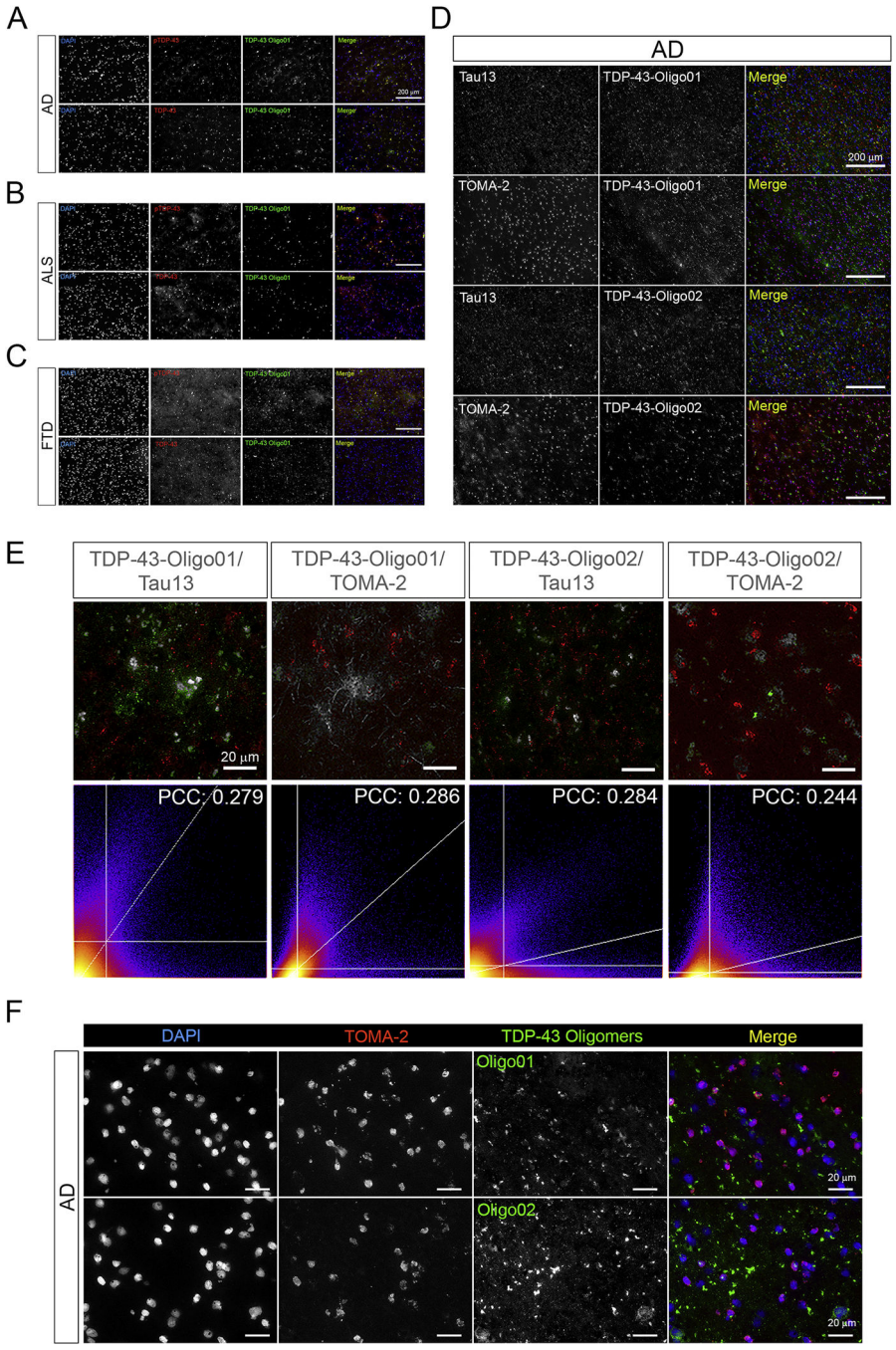

Figure 6. TDP-43Os poorly co-localize with oligomeric tau structures in AD brain tissue.

Representative images of co-staining with TDP-43/pTDP-43 (red) with TDp-43-Oligo01 (green) in AD **(A)**, ALS **(B)**, and FTD **(C)**. **(D)** Representative IF images of co-staining with Tau13/TOMA-2 (red) and TDP-43-Oligo01/02 (green) in AD tissue. **(E)** Co-localization pixel map (zoomed images) of TDP-43-Oligo01/02 with Tau13 and TOMA-2 represented in grey. Respective pixel scatter plots and PCC values are presented. (Magnification: 20x and white scale bars: 200 μm). PCC values presented are average of three ROIs for each co-staining group. **(F)** Representative high magnification images of co-staining with TOMA-2/

TDP-43-Oligo01 and TOMA-2/TDP-43-Oligo02 in AD frontal cortex. TOMA-2 (red in merge) and TDP-43-Oligo Abs (green in merge) are shown in gray in single channel images, merge is presented. Nuclei are stained with DAPI (blue). (Magnification: 100x, white scale bar: 20 μm).

Table 1.

Human brains used for this study.

Clinical diagnosis	Age	Sex	PMI (h)	Braak tangles (0–6)
ALS	64	M	17	1
ALS	68	M	24	1
ALS	84	M	30	0
FTD	56	F	21	0
FTD	60	M	7	0
AD	83	F	4.75	6
AD	86	M	3.25	6
AD	81	F	2.75	5
Control	88	M	12	1
Control	84	F	2.50	0
Control	79	M	1.75	2

Table 2

Mander's Overlap Coefficient (Average)

Abs Combinations	M(green)	M(red)
6E10 (green)+A11 (red)	0.84681	0.99873
OC (green)+A11(red)	0.98088	0.98706
Tau13 (green)+A11 (red)	0.9818	0.66047
TDP-43 Oligo01 (green)+A11 (red)	0.71793	0.9999
TDP-43 Oligo02 (green)+A11 (red)	0.74792	0.99998

Table 3.

List of Reagents and Resources

REAGENT or RESOURCE	SOURCE	IDENTIFIER
Antibodies		
TDP-43-Oligo01	In House	In House
TDP-43-Oligo02	In House	In House
A11	In House	In House
OC	In House	In House
TDP-43	Abcam	ab109535
pTDP-43	CosmoBio	TIP-PTD-M01
TDP-43 – Alexa Fluor 568	Abcam	ab208544
Tau13	BioLegend	MMS-520R
Tau5	BioLegend	806402
TOMA-2	In House	In House
6E10	BioLegend	803002
GAPDH	Abcam	ab9485
LaminB1	Abcam	ab133741
Histone3	Abcam	ab201456
Alexa Fluor Anti-Mouse 488	Invitrogen	A11029
Alexa Fluor Anti-Rabbit 488	Invitrogen	A11034
Alexa Fluor Anti-Rabbit 568	Invitrogen	A11036
Alexa Fluor Anti-Mouse 568	Invitrogen	A11031
Chemicals, Peptides, and Recombinant Proteins		
DMEM	Gibco	11965–092
Antibiotics	Gibco	15240–062
FBS	Gibco	16000–044
Paraformaldehyde, 4%	Electron Microscopy Sciences	15714-S
Triton-X 100	Sigma	T8787
Protease Inhibitor	Thermo Scientific	A32953
Tween	Fisher Scientific	BP337–500
FBS-depleted DMEM	Gibco	LS11965118
PBS	Corning	46–013-CM
Gibco™ Trypsin-EDTA, 0.25% Phenol red	Fisher Scientific	LS25200114
Goat serum	Sigma	G90223–10mL
Accutase	Sigma-Aldrich	A6964–100ML
B27 Supplemental	Gibco	A3582801
Amphotericin B	Gibco	15290018
Neurobasal™ medium	Gibco	12348017
L-glutamine	Hyclone	SH30034.01
Critical Commercial Assays		

REAGENT or RESOURCE	SOURCE	IDENTIFIER
Qproteome Cell Compartment Kit	Qiagen	#37502
Alexa Fluor™ 568 NHS Ester	Invitrogen	A20003
Lipofectamine™ RNAiMAX Transfection Reagent	Thermo Scientific	13778030
Pierce™ Co-Immunoprecipitation Kit	Thermo Scientific	#26149
Micro BCA Kit	Thermo Scientific	#23235
Experimental Models: Cell Lines		
HEK-293	Dr. Laura Blair	
WT-6 tau iHEK	Dr. Laura Blair	
P301L tau iHEK	Dr. Laura Blair	
Software and Algorithms		
GraphPad Prism 6	Graphpad.com	
ImageJ FIJI	ImageJ	NIH
Analyzer BZ-X	Keyence Microscope	Keyence Company
Other		
10kDa Amicon Ultra-0.5 Centrifugal Filter Units	Millipore	UFC501096
ProLong™ Gold Antifade Mountant with DAPI	Invitrogen	P36962